₁ The dynamics of starvation and recovery

₂ **Justin D. Yeakel** * † ‡ §, **Christopher P. Kempes** † ‡ , **and Sidney Redner** † ¶ ‡

₃ *School of Natural Science, University of California Merced, Merced, CA,†The Santa Fe Institute, Santa Fe, NM,¶Department of Physics, Boston University, Boston
₄ MA,‡Contributed equally, and §To whom correspondence should be addressed: jdyeakel@gmail.com

₆ **The eco-evolutionary dynamics of species are fundamentally**
₇ **linked to the energetic constraints of its constituent individuals.**
₈ **Of particular importance are the tradeoffs between reproduction**
₉ **and the dynamics of starvation and recovery in resource-limited**
₁₀ **environments. To elucidate the consequences of this tradeoff,**
₁₁ **we introduce a minimal nutritional state-structured model that in-**
₁₂ **corporates two classes of consumer: nutritionally replete con-**
₁₃ **sumers that reproduce, and undernourished, non-reproducing**
₁₄ **consumers that are susceptible to mortality. As a function of**
₁₅ **the transition rates between these two states that are determined**
₁₆ **by the abundance of resources, the consumer populations can ei-**
₁₇ **ther undergo cyclic dynamics or reach a steady state. We obtain**
₁₈ **strong constraints on starvation and recovery rates by deriving**
₁₉ **allometric scaling relationships between body size and a variety**
₂₀ **of traits and find that population dynamics subject to these con-**
₂₁ **straints are typically driven to a steady state. Moreover, we find**
₂₂ **that these rates fall within a 'refuge' in parameter space, where**
₂₃ **the probability of extinction of the consumer population is min-**
₂₄ **imized. Thus we identify a potential mechanism that may both**
₂₅ **drive and constrain the dynamics of animal populations. Our**
₂₆ **model provides a natural framework that predicts maximum body**
₂₇ **size for mammals by determining the relative stability of an oth-**
₂₈ **erwise homogeneous population to a mutant population with al-**
₂₉ **tered percentage of body fat. For body masses $< 1.748 \times 10^7$g,**
₃₀ **individuals with increased energetic reserves can invade resident**
₃₁ **populations, and vice versa for body mass $> 1.748 \times 10^7$g, thus**
₃₂ **providing a principled mechanism for a within-lineage driver of**
₃₃ **Cope's rule.**

₃₄ foraging | starvation | reproduction

₃₅ **Significance Statement** Energetic investment in somatic mainte-
₃₆ nance and growth vs. reproduction directly impacts the dynamics of
₃₇ populations among species. Here, we construct a Nutritional State-
₃₈ structured Model (NSM) to assess the population-level effects of star-
₃₉ vation and recovery of a consumer population in a resource-limited en-
₄₀ vironment, and use allometric scaling relationships for mammals to es-
₄₁ tablish all timescales and rates. Our model: i. reveals that mammalian
₄₂ energetic rates minimize the probability of stochastic extinction, ii. es-
₄₃ tablishes dynamic bounds on mammalian body size while providing
₄₄ independent theoretical support for the energy equivalence hypothesis,
₄₅ and iii. provides a mechanistic driver for the evolutionary trend towards
₄₆ larger body size known as Cope's rule.

₄₇ Introduction

₄₈ The behavioral ecology of all organisms is influenced by the en-
₄₉ ergetic state of individuals, which directly influences how they
₅₀ invest reserves in uncertain environments. Such behaviors are
₅₁ generally manifested as tradeoffs between investing in somatic
₅₂ maintenance and growth, or allocating energy towards repro-
₅₃ duction (1–3). The timing of these behaviors responds to se-
₅₄ lective pressure, as the choice of the investment impacts future
₅₅ fitness (4–6). The influence of resource limitation on an or-
₅₆ ganism's ability to maintain its nutritional stores may lead to
₅₇ repeated delays or shifts in reproduction over the course of an
₅₈ organism's life.
₅₉ The balance between (a) somatic growth and maintenance,
₆₀ and (b) reproduction depends on resource availability (7). For
₆₁ example, reindeer invest less in calves born after harsh winters
₆₂ (when the mother's energetic state is depleted) than in calves
₆₃ born after moderate winters (8). Many bird species invest dif-

₆₄ ferently in broods during periods of resource scarcity compared
₆₅ to normal periods (9, 10), sometimes delaying or even foregoing
₆₆ reproduction for a breeding season (1, 11, 12). Even fresh-
₆₇ water and marine zooplankton have been observed to avoid
₆₈ reproduction under nutritional stress (13), and those that do
₆₉ reproduce have lower survival rates (2). Organisms may also
₇₀ separate maintenance and growth from reproduction over space
₇₁ and time: many salmonids, birds, and some mammals return to
₇₂ migratory breeding grounds to reproduce after one or multiple
₇₃ seasons in resource-rich environments where they accumulate
₇₄ nutritional reserves (14–16).
₇₅ Physiology also plays an important role in regulating repro-
₇₆ ductive expenditures during periods of resource limitation. The
₇₇ data collected thus far has shown that diverse mammals (47
₇₈ species in 10 families) exhibit delayed implantation, whereby
₇₉ females postpone fetal development (blastocyst implantation)
₈₀ until nutritional reserves can be accumulated (17, 18). Many
₈₁ other species (including humans) suffer irregular menstrual cy-
₈₂ cling and higher abortion rates during periods of nutritional
₈₃ stress (19, 20). In the extreme case of unicellular organisms,
₈₄ nutrition is unavoidably linked to reproduction because the nu-
₈₅ tritional state of the cell regulates all aspects of the cell cycle
₈₆ (21). The existence of so many independently evolved mecha-
₈₇ nisms across such a diverse suite of organisms highlights the im-
₈₈ portance and universality of the fundamental tradeoff between
₈₉ somatic and reproductive investment. However the general dy-
₉₀ namic implications of these constraints are unknown.
₉₁ Though straightforward conceptually, incorporating the en-
₉₂ ergetic dynamics of individuals (22) into a population-level
₉₃ framework (22, 23) presents numerous mathematical obsta-
₉₄ cles (24). An alternative approach involves modeling the
₉₅ macroscale relations that guide somatic versus reproductive
₉₆ investment in a consumer-resource system. For example,
₉₇ macroscale Lotka-Volterra models assume that the growth rate
₉₈ of the consumer population depends on resource density, thus
₉₉ *implicitly* incorporating the requirement of resource availability
₁₀₀ for reproduction (25).
₁₀₁ In this work, we adopt an alternative approach in which we
₁₀₂ *explicitly* account for resource limitation and the subsequent
₁₀₃ effects of starvation. Namely, only individuals with sufficient
₁₀₄ energetic reserves can reproduce. Such a constraint leads to
₁₀₅ reproductive time lags due to some members of the population
₁₀₆ going hungry and then recovering. Additionally, we incorporate
₁₀₇ the idea that reproduction is strongly constrained allometrically
₁₀₈ (3), and is not generally linearly related to resource density. As

Reserved for Publication Footnotes

109 we shall show, these constraints influence the ensuing popula-
110 tion dynamics in dramatic ways.

111

Nutritional state-structured model (NSM)

113 We begin by defining a minimal Nutritional State-structured
114 population Model (NSM), where the consumer population is
115 partitioned into two states: (a) an energetically replete (full)
116 state F, where the consumer reproduces at a constant rate λ
117 and does not die from starvation, and (b) an energetically defi-
118 cient (hungry) state H, where the consumer does not reproduce
119 but dies by starvation at rate μ. The underlying resource R
120 evolves by logistic growth with an intrinsic growth rate α and
121 a carrying capacity C. The rate at which consumers transition
122 between states and consume resources is dependent on their
123 overall abundance, the abundance of resources, the efficiency of
124 converting resources into metabolism, and how that metabolism
125 is partitioned between maintenance and growth purposes. In
126 the supplementary information (SI) we provide a fully mecha-
127 nistic model for each of these dynamics and constants, and show
128 that the system produces a simple non-dimensional form which
129 we describe below.

130   Consumers transition from the full state F to the hungry
131 state H at a rate σ—the starvation rate—and also in propor-
132 tion to the absence of resources $(1-R)$. Conversely, consumers
133 recover from state H to state F at rate $\xi\rho$ and in proportion to
134 R, where ξ represents a ratio between maximal resource con-
135 sumption and the carrying capacity of the resource. Resources
136 are eaten by the hungry consumers at rate $\rho R+\delta$, that accounts
137 for their somatic growth (ρR) and maintenance (δ). Full con-
138 sumers eat resources at a constant rate β that accounts for max-
139 imal maintenance and somatic growth (see SI for mechanistic
140 derivations of these rates from resource energetics). The NSM
141 represents an ecologically motivated fundamental extension of
142 the idealized starving random walk model of foraging, which
143 focuses on resource depletion, to include reproduction and re-
144 source replenishment (26–28), and is a more general formulation
145 than previous models incorporating starvation (29).

146   In the mean-field approximation, in which the consumers
147 and resources are perfectly mixed, their densities evolve accord-
148 ing to the rate equations

$$\frac{dF}{dt} = \lambda F + \xi\rho R H - \sigma(1-R)F,$$
$$\frac{dH}{dt} = \sigma(1-R)F - \xi\rho R H - \mu H, \qquad [\mathbf{1}]$$
$$\frac{dR}{dt} = \alpha(1-R)R - (\rho R + \delta)H - \beta F$$

149   This system of nondimensional equations follows from a
150 set of first-principle relationships for resource consumption and
151 growth (see SI for a full derivation and the dimensional form).
152 Notice that the total consumer density $F + H$ evolves accord-
153 ing to $\frac{dF}{dt} + \frac{dH}{dt} = \lambda F - \mu H$. This resembles the equation of
154 motion for the predator density in the classic Lotka-Volterra
155 model (30), except that the resource density does not appear in
156 the growth term. As discussed above, the attributes of repro-
157 duction and mortality have been explicitly apportioned to the
158 full and hungry consumers, respectively, so that the growth in
159 the total density is decoupled from the resource density.

    Equation [$\mathbf{1}$] has three fixed points: two trivial fixed points
at $(F^*, H^*, R^*) = (0, 0, 0)$ and $(0, 0, 1)$, and one non-trivial,
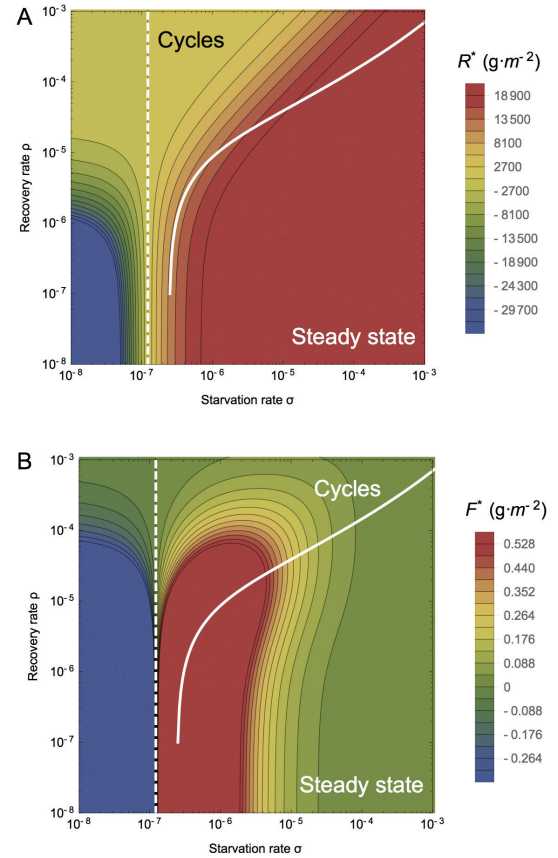
Fig. 1: The transcritical (dashed) and Hopf bifurcation (solid) as a function of the starvation rate σ and recovery rate ρ for a 100g consumer. These bifurcation conditions separate parameter space into unphysical, cyclic, and steady state dynamic regimes. The colors show the steady state densities for (A) the resource R^* and the (B) energetically replete consumers F^*, (warmer colors denote higher densities). Steady state densities for the energetically deficient consumers H^* (not shown) scale with those for F^*.

internal fixed point at

$$F^* = (\sigma - \lambda)\frac{\alpha\lambda\mu^2(\mu + \xi\rho)}{A(\lambda\rho B + \mu\sigma(\beta\mu + \lambda(\delta + \rho)))},$$
$$H^* = (\sigma - \lambda)\frac{\alpha\lambda^2\mu(\mu + \xi\rho)}{A(\lambda\rho B + \mu\sigma(\beta\mu + \lambda(\delta + \rho)))}, \qquad [\mathbf{2}]$$
$$R^* = (\sigma - \lambda)\frac{\mu}{A}.$$

160 where $A = (\lambda\xi\rho + \mu\sigma)$ and $B = (\beta\mu\xi + \delta\lambda\xi - \lambda\mu)$. The sta-
161 bility of this fixed point is determined by the Jacobian matrix
162 $\mathbf{J}$, where each matrix element $J_{ij} = \partial\dot{X}_i/\partial X_j$ when evaluated
163 at the internal fixed point, and $\mathbf{X}$ is the vector (F, H, R). The
164 parameters in Eq. [$\mathbf{1}$] are such that the real part of the largest
165 eigenvalue of $\mathbf{J}$ is negative, so that the system is stable with
166 respect to small perturbations from the fixed point. Because
167 this fixed point is unique, it is the global attractor for all pop-
168 ulation trajectories for any initial condition where the resource
169 and consumer densities are both nonzero.

170   From Eq. [$\mathbf{2}$], an obvious constraint on the NSM is that
171 the reproduction rate λ must be less than the starvation rate
172 σ, so that the consumer and resource densities are positive.
173 The condition $\sigma = \lambda$ thus represents a transcritical (TC) bi-
174 furcation (31) that demarcates a physical from an unphysical
175 regime where all steady-state densities become negative after in-
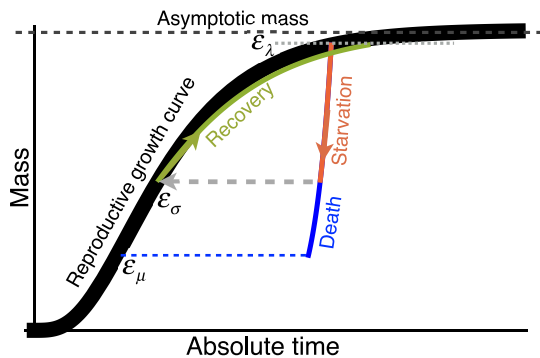176 tersecting the trivial fixed point $(F^*, H^*, R^*) = (0, 0, 0)$. The

biological implication of the constraint $\lambda < \sigma$ has a simple interpretation—the rate at which a macroscopic organism loses mass due to lack of resources is generally much faster than the rate of reproduction. As we will discuss below, this inequality is a natural consequence of allometric constraints (3) for organisms within empirically observed body size ranges.

In the physical regime of $\lambda < \sigma$, the fixed point [2] may either be a stable node or a limit cycle (Fig.). In continuous-time systems, a limit cycle arises when a pair of complex conjugate eigenvalues crosses the imaginary axis to attain positive real parts (32). This Hopf bifurcation is defined by $\text{Det}(\mathbf{S}) = 0$, with $\mathbf{S}$ the Sylvester matrix, which is composed of the coefficients of the characteristic polynomial of the Jacobian matrix (33). As the system parameters are tuned to be within the stable regime, but close to the Hopf bifurcation, the amplitude of the transient cycles becomes large. Given that ecological systems are constantly being perturbed (34), the onset of transient cycles, even though they decay with time in the mean-field description, can increase the extinction risk (35–37).

When the starvation rate $\sigma \gg \lambda$, a substantial fraction of the consumers are driven to the hungry non-reproducing state. Because reproduction is inhibited, there is a low steady-state consumer density and a high steady-state resource density. However, if $\sigma/\lambda \to 1$ from above, the population is overloaded with energetically-replete (reproducing) individuals, thereby promoting transient oscillations between the consumer and resource densities (Fig.). If the starvation rate is low enough that the Hopf bifurcation is crossed, these oscillations become stable over time. This threshold occurs at higher values of the starvation rate as the recovery rate ρ increases, such that the range of parameter space giving rise to cyclic dynamics also increases with higher recovery rates.

Role of allometry

While there are no a priori constraints on the parameters in the NSM, most organisms correspond to restricted portions of the parameter space. Here we use allometric scaling relations to constrain the covariation of rates in a principled and biologically meaningful manner. Allometric scaling relations highlight common constraints and average trends across large ranges in body size and species diversity. Many of these relations can be derived from a small set of assumptions and below we describe our framework to determine the covariation of timescales and rates across the range of mammals for each of the key parameters of our model (cf. ref. 38). We are thereby able to define the regime of dynamics occupied by the entire class of mammals, along with the key differences between the largest and smallest mammals.

Nearly all of the rates described in the NSM are determined by consumer metabolism, which can be used to describe a variety of organismal features (39). The scaling relation between an organism's metabolic rate B and its body mass M at reproductive maturity is known to scale as $B = B_0 M^\eta$ (40), where the scaling exponent η is typically close to 2/3 or 3/4 for metazoans (e.g., ref. 39), and has taxonomic shifts for unicellular species between $\eta \approx 1$ in eukaryotes and $\eta \approx 1.76$ in bacteria (3, 41).

Several efforts have shown how a partitioning of B between growth and maintenance purposes can be used to derive a general equation for both the growth trajectories and growth rates of organisms ranging from bacteria to metazoans (3, 42–45). This relation is derived from the simple balance condition $B_0 m^\eta = E_m \dot{m} + B_m m$, (3, 42–45) where E_m is the energy needed to synthesize a unit of mass, B_m is the metabolic rate to support an existing unit of mass, and m is the mass of the organism at any point in its development. This balance has the general solution (3, 46)

$$\left(\frac{m(t)}{M}\right)^{1-\eta} = 1 - \left[1 - \left(\frac{m_0}{M}\right)^{1-\eta}\right] e^{-a(1-\eta)t/M^{1-\eta}}, \qquad [3]$$
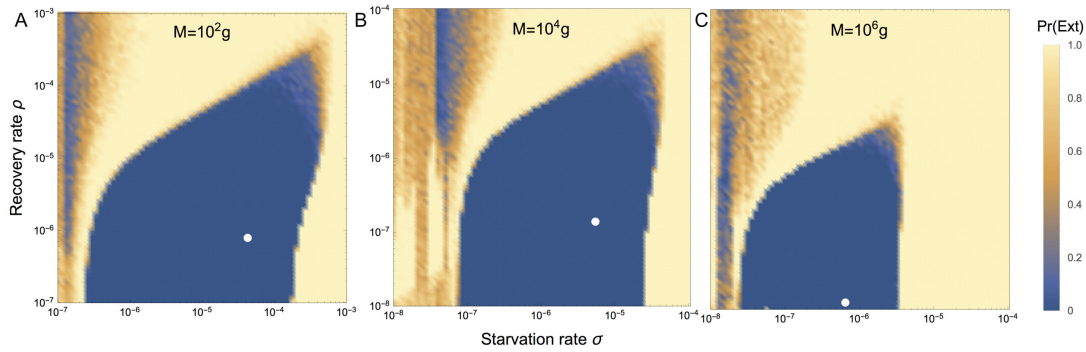
where, for $\eta < 1$, $M = (B_0/B_m)^{1/(1-\eta)}$ is the asymptotic mass, $a = B_0/E_m$, and m_0 is mass at birth, itself varying allometrically (see SI). We now use this solution to define the timescale for reproduction and recovery from starvation (Fig. 7; see (43) for a detailed presentation of these timescales). The time that it takes to reach a particular mass ϵM is given by the timescale

$$\tau(\epsilon) = \ln\left[\frac{1 - (m_0/M)^{1-\eta}}{1 - \epsilon^{1-\eta}}\right] \frac{M^{1-\eta}}{a(1-\eta)}, \qquad [4]$$

where we will define values of ϵ to describe a set of rates within our model. For the time to reproduce, $t_\lambda = \tau(\epsilon_\lambda)$, where ϵ_λ is the fraction of the asymptotic mass where an organism is reproductively mature and should be close to one (typically $\epsilon_\lambda \approx 0.95$; 42). The growth rate is then given by $\lambda = \ln(\upsilon)/t_\lambda$ where υ is the number of offspring produced, and for any constant value of ϵ_λ, this rate will scale as $\lambda \propto M^{\eta-1}$ for $M \gg m_0$ (3, 42–45).

The rate of recovery $\rho = 1/t_\rho$ requires that an organism accrues sufficient tissue to transition from the hungry to the full state. Since only certain tissues can be digested for energy (for example the brain cannot be degraded to fuel metabolism), we define the rates for starvation, death, and recovery by the timescales required to reach, or return from, specific fractions of the replete-state mass (Fig. ??; see SI, Table I for parameterizations). We define $m_\sigma = \epsilon_\sigma M$, where $\epsilon_\sigma < 1$ is the fraction of replete-state mass where reproduction ceases. This fraction will deviate from a constant if tissue composition systematically scales with adult mass. For example, making use of the observation that body fat in mammals scales with overall body size according to $M_{\text{fat}} = f_0 M^\gamma$ and assuming that once this mass is fully digested the organism starves, this would imply $\epsilon_\sigma = 1 - f_0 M^\gamma/M$. It follows that the recovery timescale, t_ρ, is the time to go from $m = \epsilon_\sigma \epsilon_\lambda M$ to $m = \epsilon_\lambda M$ (Fig. 7). Using Eqs. [3] and [4] this timescale is given by simply considering an adjusted starting mass of $m'_0 = \epsilon_\sigma \epsilon_\lambda M$, in which case

$$t_\rho = \ln\left[\frac{1 - (\epsilon_\sigma \epsilon_\lambda)^{1-\eta}}{1 - \epsilon_\lambda^{1-\eta}}\right] \frac{M^{1-\eta}}{a'(1-\eta)} \qquad [5]$$

Fig. 2: The growth trajectory over absolute time of an individual organism as a function of body mass. Initial growth follows the black trajectory to an energetically replete reproductive adult mass $m = \epsilon_\lambda M$ which we assume is 95% asymptotic mass M. Starvation follows the red trajectory to $m = \epsilon_\sigma \epsilon_\lambda M$. Recovery follows the green curve to the replete adult mass, where this trajectory differs from the original growth because only fat is being regrown which requires different energetics and a longer time to reach $\epsilon_\lambda M$. Alternatively, death from starvation follows the blue trajectory to $m = \epsilon_\mu \epsilon_\lambda M$.

Fig. 3: Probability of extinction for a consumer with (A) $M = 10^2$g, (B) $M = 10^4$g, and (C) $M = 10^6$g as a function of the starvation rate σ and recovery rate ρ, where the initial density is given as (XF^*, XH^*, R^*), where X is a random uniform variable in $[0, 2]$. Note the change in scale for $M = 10^4$ and $M = 10^6$g. Extinction is defined as the population trajectory falling below $0.2\times$ the allometrically constrained steady state. The white points denote the allometrically constrained starvation and recovery rate.

where $a' = B_0/E'_m$ accounts for possible deviations in the biosynthetic energetics during recovery (see SI). It should be noted that more complicated ontogenetic models explicitly handle storage (45), whereas this feature is implicitly covered by the body fat scaling in our framework.

To determine the starvation rate, σ, we are interested in the time required for an organism to go from a mature adult that reproduces at rate λ, to a reduced-mass hungry state where reproduction is impossible. For starving individuals we assume that an organism must meet its maintenance requirements by using the digestion of existing mass as the sole energy source. This assumption implies the following simple metabolic balance $\dot{m}E'_m = -B_m m$ or $\dot{m} = -a'm/M^{1-\eta}$ where E'_m is the amount of energy stored in a unit of existing body mass, which differs from E_m, the energy required to synthesis a unit of biomass (45). Given the replete mass, M, of an organism, the above energy balance prescribes the mass trajectory of a non-consuming organism:$m(t) = Me^{-a't/M^{1-\eta}}$. The timescale for starvation is given by the time it takes $m(t)$ to reach $\epsilon_\sigma M$, which gives

$$t_\sigma = -\frac{M^{1-\eta}}{a'} \ln(\epsilon_\sigma). \qquad [6]$$

The starvation rate is then $\sigma = 1/t_\sigma$, which scales with replete-state mass as $1/M^{1-\eta} \ln(1 - f_0 M^\gamma/M)$. An important feature is that σ does not have a simple scaling dependence on λ (Fig. **??**), which is important for the dynamics that we later discuss.

The time to death should follow a similar relation, but defined by a lower fraction of replete-state mass, $m_\mu = \epsilon_\mu M$ where $\epsilon_\mu < \epsilon_\sigma$. Suppose, for example, that an organism dies once it has digested all fat and muscle tissues, and that muscle tissue scales with body mass according to $M_{\text{musc}} = u_0 M^\zeta$. This gives $\epsilon_\mu = 1 - (f_0 M^\gamma + u_0 M^\zeta)/M$. Muscle mass has been shown to be roughly proportional to body mass (47) in mammals and thus ϵ_μ is merely ϵ_σ minus a constant. The time to go from starvation to death is the total time to reach $\epsilon_\mu M$ minus the time to starve, or

$$t_\mu = -\frac{M^{1-\eta}}{a'} \ln(\epsilon_\mu) - t_\sigma, \qquad [7]$$

and $\mu = 1/t_\mu$.

Although the rate equations [1] are general, here we focus on parameterizations for terrestrial-bound endotherms, specifically mammals, which range from a minimum of $M \approx 1$g (the Etruscan shrew *Suncus etruscus*) to a maximum of $M \approx 10^7$g (the early Oligocene Indricotheriinae and the Miocene Deinotheriinae). Investigating other classes of organisms would simply involve altering the metabolic exponents and scalings

associate with ϵ. Moreover, we emphasize that our allometric equations describe mean relationships, and do not account for the (sometimes considerable) variance associated with individual species.

Stabilizing effects of allometric constraints

As the allometric derivations of the NSM rate laws reveal, starvation and recovery rates are not independent parameters, and the biologically relevant portion of the phase space shown in Fig. is constrained via covarying parameters. Given the parameters of terrestrial endotherms, we find that the starvation rate σ and the recovery rate ρ are constrained to lie within a small region of potential values (Fig. **??**) for the known range of body sizes M. We thus find that the dynamics for all mammalian body sizes are confined to the steady-state regime of the NSM and that limit-cycle behavior is precluded. Incorporating uncertainty in allometric parameters (20% variation around the mean; Fig. **??**), we find that, for larger M, the distance to the TC and Hopf bifurcation decreases. These results suggest that small mammals are marginally less prone to population oscillations—both stable limit cycles and transient cycles—than mammals with larger body size. However, starvation and recovery rates across all values of M fall squarely in the steady state region at some distance from the Hopf bifurcation. This result suggests that cyclic population dynamics should be rare, particularly in environments where resources are limiting.
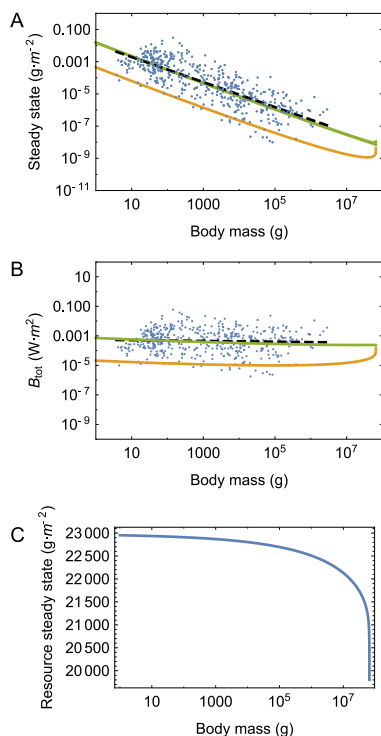
Extinction risk

Within our model, higher rates of starvation result in a larger flux of the population to the hungry state. In this state, reproduction is absent, thus increasing the likelihood of extinction. From the perspective of population survival, it is the rate of starvation relative to the rate of recovery that determines the long-term dynamics of the various species (Fig.). We therefore examine the competing effects of cyclic dynamics vs. changes in steady-state density on extinction risk, both as functions of σ and ρ. To this end, we computed the probability of extinction, where we define extinction as a population trajectory falling below one fifth of the allometrically constrained steady state at any time between $t = 10^8$ and $t = 10^{10}$. This procedure is repeated for 50 replicates of the continuous-time system shown in Eq. 1 for organisms with mass ranging from 10^2 to 10^6 grams. In each replicate the initial densities are chosen to be (XF^*, XH^*, R^*), with X a random variable that is uniformly distributed in $[0, 2]$. By allowing the rate of starvation to vary, we assessed extinction risk across a range of values for σ and ρ between ca. 10^{-7} to 10^{-3}. As expected, higher rates of extinction correlate with both high values of σ if ρ is small, and high

values of ρ if σ is small. For low values of σ and high values of ρ, the increased extinction risk results from transient cycles with larger amplitudes as the system nears the Hopf bifurcation (Fig. 3). For high values of σ and low values of ρ, increased extinction risk arises because of the decrease in the steady-state consumer population density (Figs. B, 3). This interplay creates an 'extinction refuge', such that for a constrained range of σ and ρ, extinction probabilities are minimized.

We find that the allometrically constrained values of σ and ρ fall squarely within the extinction refuge across a range of M (Fig. 3A-C, white points). These values are close enough to the Hopf bifurcation to avoid low steady-state densities, and far enough away to avoid large-amplitude transient cycles. The feature that allometric values of σ and ρ fall within this relatively small window supports the possibility that a selective mechanism has constrained the physiological conditions that drive starvation and recovery rates within populations. Such a mechanism would select for organism physiology that generates appropriate σ and ρ values that serve to minimize extinction risk. This selection could occur via the tuning of body fat percentages, metabolic rates, and biomass maintenance efficiencies. We also find that as body size increases, the amount of low extinction risk parameter space becomes smaller (Fig. 3A-C), suggesting that the population dynamics of larger organisms are more sensitive to smaller changes in physiological rates controlling starvation and recovery. To summarize, our finding that the allometrically-determined parameters fall within this low extinction probability region suggests that the NSM dynamics may both drive—and constrain—natural animal populations.

Dynamic and energetic barriers to body size

Metabolite transport constraints are widely thought to place strict boundaries on biological scaling (39, 55, 56) and thereby lead to specific predictions on the minimum possible body size for organisms (57). Above this bound, a number of energetic and evolutionary mechanisms have been explored to assess the costs and benefits associated with larger body masses, particularly for mammals. One important such example is the *fasting endurance hypothesis*, which contends that larger body size, with consequent lower metabolic rates and increased ability to maintain more endogenous energetic reserves, may buffer organisms against environmental fluctuations in resource availability (58). Over evolutionary time, terrestrial mammalian lineages show a significant trend towards larger body size (known as Cope's rule) (59–62), and it is thought that within-lineage drivers generate selection towards an optimal upper bound of roughly 10^7 grams (59), a value that is likely limited by higher extinction risk for large taxa over longer timescales (60). These trends are thought to be driven by a combination of climate change and niche availability (62); however the underpinning energetic costs and benefits of larger body sizes, and how they influence dynamics over ecological timescales, have not been explored. We argue that the NSM provides a suitable framework to explore these issues.

The NSM correctly predicts that species with smaller masses have larger steady-state population densities (Fig. 3A). Moreover, we show that the NSM provides independent theoretical support for the energy equivalence hypothesis and Damuth's Law (63–65). The energy equivalence hypothesis argues that the total energy use, B_{tot}, of a population is constant independent of species size (63–65). This hypothesis is based on observations showing that the steady state abundance, N^*, of a species is proportional to the inverse of individual metabolism, such that $N^* \propto M^{-3/4}/B_0$ (64, 65). This relationship implies that $B_{\mathrm{tot}} = N^*B(M) = Q$, where Q is a constant, and has been shown to hold in both mammalian and vascular plant communities (63–65). Figure 3A shows that both F^* and H^* scale as $M^{-\eta}$ over a wide range of organism sizes and Figure 3B shows that F^*B is nearly constant over this same range. This result is remarkable because it illustrates that the steady state values of the NSM combined with the derived timescales naturally give rise to energy equivalence. Our model shows that the equivalence breaks down at the maximum observed body sizes for mammals, suggesting that this maximum is a hard limit where deviations outside of this range are energetically suboptimal. In the framework of our model, the total metabolic rate of F and H becomes infinite at a finite mass, and occur at the same scale where the steady state resources vanish (Fig. 3). This asymptotic behavior is governed by body sizes at which ϵ_μ and ϵ_λ equal zero causing the timescales to become infinite (see Equation 3) and the rates μ and λ to equal zero. The $\mu = 0$ asymptote occurs first when $f_0 M^{\gamma-1} + u_0 M^{\zeta-1} = 1$, and corresponds to $(F^*, H^*, R^*) = (0, 0, 0)$. This point predicts a strong upper bound on mammalian body size and occurs at $M_{\mathrm{max}} = 6.54 \times 10^7$. Moreover, M_{max}, which is entirely determined by the population-level consequences of energetic constraints, is close to the maximum body size observed in the North American mammalian fossil record (59), as well as the mass predicted from an evolutionary model of body size evolution (60). It should be noted that the asymptotic behavior and predicted upper bound depend only on the scaling of body composition and are independent of the resource parameters. We also note that the prediction of an asymptotic limit on mammalian size parallels work on microbial life where an upper and lower bound on bacterial size, and an upper bound on single cell eukaryotic size, is predicted from similar growth and energetic scaling relationships (3, 66).

Fig. 4: (A) Consumer steady states F^* (green) and H^* (orange) as a function of body mass. (B) Total energetic use B_{tot} of consumer populations at the steady state as a function of body mass. (C) Resource steady state R^* as a function of consumer body mass. The data are from Damuth (63) and have been converted to total population metabolism using the allometric relationships for metabolic rate (please see SI and Refs. 42, 43, 45).

We contend that the NSM provides a mechanistic understanding of the energetic dynamics that give rise to both observed limitations on mammalian body size, as well as the observed trend towards larger body size over evolutionary time. The NSM predicts that the steady state resource density R^* decreases with increasing body size of the consumer population (Fig. 3C), and classic resource competition theory predicts that the species surviving on the lowest resource abundance will outcompete others (67–69). Thus, the combined NSM steady-state dynamics and allometric timescales predict that larger mammals have an intrinsic competitive advantage given a common resource, but does not offer a within-lineage mechanism by which larger body sizes are selected for.

To examine whether the NSM could provide such a mechanism, we begin by noting that a theoretical upper bound on mammalian body size is given by $\epsilon_\sigma = 0$, where mammals are entirely composed of metabolic reserves, and this occurs at $M = 8.3 \times 10^8$, or 120 times the mass of a male African elephant. Next we examine to what extent a more realistic upper bound to body mass may serve as an evolutionary attractor, thus providing a suitable within-lineage mechanism for Cope's rule. We directly assess the susceptibility of an otherwise homogeneous population to invasion by a mutated subset of the population (denoted by $'$) where individuals have a modified proportion of body fat $M' = M(1+\chi)$. For the allowable values of χ the adjusted mass should exceed the amount of body fat, $1+\chi > \epsilon_\sigma$, and the adjusted time to reproduce must be positive, which given Equation 4, implies that $1 - \epsilon_\lambda^{1-\eta}(1+\chi)^{1-\eta} > 0$. Together these conditions imply that $\chi \in (-f_0 M^{\gamma-1}, 1/\epsilon_\lambda - 1)$ where the upper bound approximately equals 0.05. The modified mass adjusts our model via the altered rates of starvation $\sigma(M')$, recovery $\rho(M')$, and the maintenance of both starving $\delta(M')$ and full consumers $\beta(M')$. Importantly, ϵ_σ, which determines the point along the growth curve that defines the body composition of starved foragers, is assumed to remain unchanged for the invader population (see SI for detailed derivations of invader rates).

To assess the susceptibility of the resident population to invasion, we determine which consumer has a lower steady-state resource density for a given value of χ, again with the expectation that populations able to survive on lower resource densities have a competitive advantage (67). We find that for $M \le 1.748 \times 10^7$g, having additional body fat ($\chi > 0$) results in a lower steady state resource density ($R'^* < R^*$), such that the invader has an intrinsic competitive advantage over the resident population. However, for $M > 1.748 \times 10^7$g, leaner individuals ($\chi < 0$) have lower resource steady state densities, switching the advantage for higher values of M.

The observed switch in susceptibility as a function of χ at $M_{\text{opt}} = 1.748 \times 10^7$g thus serves as an attractor, such that the NSM predicts organismal mass to increase if $M < M_{\text{opt}}$ and decrease if $M > M_{\text{opt}}$. This value is close to but smaller than the asymptotic upper bound for terrestrial mammal body size predicted by the NSM, however it is remarkably close to independent estimates of the largest land mammals, the early Oligocene *Indricotherium* at ca. 1.5×10^7g and the late Miocene *Deinotherium* at ca. 1.74×10^7g (61). Additionally, our calculation of M_{opt} as a function of mass-dependent physiological rates is similar to theoretical estimates of maximum body size (60), and provides independent theoretical support for the observation of a 'maximum body size attractor' for North American mammals outlined by Alroy (59). While the state of the environment, as well as the competitive landscape, will determine whether specific body sizes are selected for or against (62), we propose that the dynamics of starvation and recovery described in the NSM provide a general within-lineage mechanism for the evolution of larger body size among terrestrial mammals.

The energetics associated with somatic maintenance, growth, and reproduction are important elements that influence the dynamics of all populations (11). The NSM is a minimal and general model that incorporates the dynamics of starvation and recovery that are expected to occur in resource-limited environments. By incorporating allometric relations between the rates in the NSM, we found: (i) different organismal masses have distinct population dynamic regimes, (ii) allometrically-determined rates of starvation and recovery appear to minimize extinction risk, and (iii) the dynamic consequences of these rates may introduce additional drivers and hard boundaries on the evolution of maximum body size. We suggest that the NSM offers a means by which the dynamic consequences of energetic constraints can be assessed using macroscale interactions between and among species. Future efforts will involve exploring the consequences of these dynamics in a spatially explicit framework, thus incorporating elements such as movement costs and spatial heterogeneity, which may elucidate additional tradeoffs associated with the dynamics of starvation and recovery.
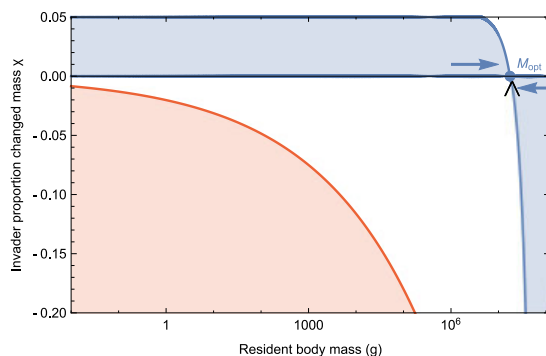
Fig. 5: Invasion feasibility for organisms with a proportional change in mass χ against a population with a resident body mass M. The blue region denotes proportions of modified mass χ resulting in successful invasion. The red region denotes values of χ that result in a mass that is below the starvation threshold and are thus infeasible. Arrows point to the predicted optimal mass from our model $M_{\text{opt}} = 1.748 \times 10^7$, which may serve as an evolutionary attractor for body mass. The black wedge points to the largest body mass known for terrestrial mammals (*Deinotherium* spp.) at 1.74×10^7g (61).

References

1. Martin TE (1987) Food as a limit on breeding birds: A life-history perspective. *Annu. Rev. Ecol. Syst.* 18:453–487.
2. Kirk KL (1997) Life-history responses to variable environments: Starvation and reproduction in planktonic rotifers. *Ecology* 78:434–441.
3. Kempes CP, Dutkiewicz S, Follows MJ (2012) Growth, metabolic partitioning, and the size of microorganisms. *Proc. Natl. Acad. Sci. USA* 109:495–500.
4. Mangel M, Clark CW (1988) *Dynamic Modeling in Behavioral Ecology* (Princeton University Press, Princeton).
5. Mangel M (2014) Stochastic dynamic programming illuminates the link between environment, physiology, and evolution. *B. Math. Biol.* 77:857–877.
6. Yeakel JD, Dominy NJ, Koch PL, Mangel M (2014) Functional morphology, stable isotopes, and human evolution: a model of consilience. *Evolution* 68:190–203.
7. Morris DW (1987) Optimal allocation of parental investment. *Oikos* 49:332–339.
8. Tveraa T, Fauchald P, Henaug C, Yoccoz NG (2003) An examination of a compensatory relationship between food limitation and predation in semi-domestic reindeer. *Oecologia* 137:370–376.
9. Daan S, Dijkstra C, Drent R, Meijer T (1989) in *Acta XIX Congressus Internationalis Ornithologici, Volume I: Proceedings XIX International Ornithological Congress, 1986, Ottawa*, ed Ouellet H (Proceedings XIX International Ornithological Congress, Ottawa), pp 392–407.
10. Jacot A, Valcu M, van Oers K, Kempenaers B (2009) Experimental nest site limitation affects reproductive strategies and parental investment in a hole-nesting passerine. *Animal Behaviour* 77:1075–1083.
11. Stearns SC (1989) Trade-offs in life-history evolution. *Funct. Ecol.* 3:259.
12. Barboza P, Jorde D (2002) Intermittent fasting during winter and spring affects body composition and reproduction of a migratory duck. *J Comp Physiol B* 172:419–434.
13. Threlkeld ST (1976) Starvation and the size structure of zooplankton communities. *Freshwater Biol.* 6:489–496.

14. Weber TP, Ens BJ, Houston AI (1998) Optimal avian migration: A dynamic model of fuel stores and site use. *Evolutionary Ecology* 12:377–401.
15. Mduma SAR, Sinclair ARE, Hilborn R (1999) Food regulates the Serengeti wildebeest: a 40-year record. *J. Anim. Ecol.* 68:1101–1122.
16. Moore JW, Yeakel JD, Peard D, Lough J, Beere M (2014) Life-history diversity and its importance to population stability and persistence of a migratory fish: steelhead in two large North American watersheds. *J. Anim. Ecol.* 83:1035–1046.
17. Mead RA (1989) in *Carnivore Behavior, Ecology, and Evolution*, ed Gittleman JL (Springer US, Ithaca), pp 437–464.
18. Sandell M (1990) The evolution of seasonal delayed implantation. *Q Rev Biol* 65:23–42.
19. Bulik CM, et al. (1999) Fertility and reproduction in women with anorexia nervosa. *J. Clin. Psychiat.* 60:130–135.
20. Trites AW, Donnelly CP (2003) The decline of Steller sea lions Eumetopias jubatus in Alaska: a review of the nutritional stress hypothesis. *Mammal Rev.* 33:3–28.
21. Glazier DS (2009) Metabolic level and size scaling of rates of respiration and growth in unicellular organisms. *Funct. Ecol.* 23:963–968.
22. Kooijman SALM (2000) *Dynamic Energy and Mass Budgets in Biological Systems* (Cambridge).
23. Sousa T, Domingos T, Poggiale JC, Kooijman SALM (2010) Dynamic energy budget theory restores coherence in biology. *Philos. T. Roy. Soc. B* 365:3413–3428.
24. Diekmann O, Metz JAJ (2010) How to lift a model for individual behaviour to the population level? *Philos. T. Roy. Soc. B* 365:3523–3530.
25. Murdoch WW, Briggs CJ, Nisbet RM (2003) *Consumer-resource Dynamics*, Monographs in population biology (Princeton University Press, Princeton) Vol. 36.
26. Benichou O, Redner S (2014) Depletion-Controlled Starvation of a Diffusing Forager. *arXiv* pp 1–5.
27. Bénichou O, Chupeau M, Redner S (2016) Role of depletion on the dynamics of a diffusing forager. *Journal of Physics A: . . . .*
28. Chupeau M, Bénichou O, Redner S (2016) Universality classes of foraging with resource renewal. *Phys. Rev. E* 93:032403.
29. Persson L, Leonardsson K, De Roos AM, Gyllenberg M, Christensen B (1998) Ontogenetic scaling of foraging rates and the dynamics of a size-structured consumer-resource model. *Theor Popul Biol* 54:270–293.
30. Murray JD (2011) *Mathematical Biology: I. An Introduction*, Interdisciplinary Applied Mathematics (Springer New York) Vol. 110.
31. Strogatz SH (2008) *Nonlinear Dynamics and Chaos: With Applications to Physics, Biology, Chemistry, and Engineering*, Studies in nonlinearity (Westview Press, Boulder).
32. Guckenheimer J, Holmes P (1983) *Nonlinear Oscillations, Dynamical Systems, and Bifurcations of Vector Fields* (Springer, New York).
33. Gross T, Feudel U (2004) Analytical search for bifurcation surfaces in parameter space. *Physica D* 195:292–302.
34. Hastings A (2001) Transient dynamics and persistence of ecological systems. *Ecol. Lett.* 4:215–220.
35. Neubert M, Caswell H (1997) Alternatives to resilience for measuring the responses of ecological systems to perturbations. *Ecology* 78:653–665.
36. Caswell H, Neubert MG (2005) Reactivity and transient dynamics of discrete-time ecological systems. *J Differ Equ Appl* 11:295–310.
37. Neubert M, Caswell H (2009) Detecting reactivity. *Ecology* 90:2683–2688.
38. Yodzis P, Innes S (1992) Body size and consumer-resource dynamics. *Am. Nat.* 139:1151–1175.
39. Brown J, Gillooly J, Allen A, Savage V, West G (2004) Toward a metabolic theory of ecology. *Ecology* 85:1771–1789.
40. West GB, Woodruff WH, Brown JH (2002) Allometric scaling of metabolic rate from molecules and mitochondria to cells and mammals. *Proc. Natl. Acad. Sci. USA* 99 Suppl 1:2473–2478.
41. DeLong JP, Okie JG, Moses ME, Sibly RM, Brown JH (2010) Shifts in metabolic scaling, production, and efficiency across major evolutionary transitions of life. *Proc. Natl. Acad. Sci. USA* 107:12941–12945.
42. West GB, Brown JH, Enquist BJ (2001) A general model for ontogenetic growth. *Nature* 413:628–631.
43. Moses ME, et al. (2008) Revisiting a Model of Ontogenetic Growth: Estimating Model Parameters from Theory and Data. *Am. Nat.* 171:632–645.
44. Gillooly JF, Charnov EL, West GB, Savage VM, Brown JH (2002) Effects of size and temperature on developmental time. *Nature* 417:70–73.
45. Hou C, et al. (2008) Energy uptake and allocation during ontogeny. *Science* 322:736–739.
46. Bettencourt LMA, Lobo J, Helbing D, Kuhnert C, West GB (2007) Growth, innovation, scaling, and the pace of life in cities. *Proc. Natl. Acad. Sci. USA* 104:7301–7306.
47. Folland JP, Mc Cauley TM, Williams AG (2008) Allometric scaling of strength measurements to body size. *Eur J Appl Physiol* 102:739–745.
48. Calder III WA (1983) An allometric approach to population cycles of mammals. *J. Theor. Biol.* 100:275–282.
49. Peterson RO, Page RE, Dodge KM (1984) Wolves, moose, and the allometry of population cycles. *Science* 224:1350–1352.
50. Krukonis G, Schaffer WM (1991) Population cycles in mammals and birds: Does periodicity scale with body size? *J. Theor. Biol.* 148:469–493.
51. Hendriks AJ, Mulder C (2012) Delayed logistic and Rosenzweig–MacArthur models with allometric parameter setting estimate population cycles at lower trophic levels well. *Ecol Complex* 9:43–54.
52. Kendall BE, et al. (1999) Why do populations cycle? A synthesis of statistical and mechanistic modeling approaches. *Ecology* 80:1789–1805.
53. Högstedt G, Seldal T, Breistol A (2005) Period length in cyclic animal populations. *Ecology* 86:373–378.
54. Kendall, Prendergast, Bjornstad (1998) The macroecology of population dynamics: taxonomic and biogeographic patterns in population cycles. *Ecol. Lett.* 1:160–164.
55. Brown J, Marquet P, Taper M (1993) Evolution of body size: consequences of an energetic definition of fitness. *Am. Nat.* 142:573–584.
56. West GB, Brown JH, Enquist BJ (1997) A general model for the origin of allometric scaling laws in biology. *Science* 276:122–126.
57. West GB, Woodruff WH, Brown JH (2002) Allometric scaling of metabolic rate from molecules and mitochondria to cells and mammals. *Proc. Natl. Acad. Sci. USA* 99 Suppl 1:2473–2478.
58. Millar J, Hickling G (1990) Fasting endurance and the evolution of mammalian body size. *Funct. Ecol.* 4:5–12.
59. Alroy J (1998) Cope's rule and the dynamics of body mass evolution in North American fossil mammals. *Science* 280:731–734.
60. Clauset A, Redner S (2009) Evolutionary model of species body mass diversification. *Phys. Rev. Lett.* 102:038103.
61. Smith FA, et al. (2010) The evolution of maximum body size of terrestrial mammals. *Science* 330:1216–1219.
62. Saarinen JJ, et al. (2014) Patterns of maximum body size evolution in Cenozoic land mammals: Eco-evolutionary processes and abiotic forcing. *Proc Biol Sci* 281:20132049.
63. Damuth J (1987) Interspecific allometry of population density in mammals and other animals: the independence of body mass and population energy-use. *Biol. J. Linn. Soc.* 31:193–246.
64. Allen AP, Brown JH, Gillooly JF (2002) Global biodiversity, biochemical kinetics, and the energetic-equivalence rule. *Science* 297:1545–1548.
65. Enquist BJ, Brown JH, West GB (1998) Allometric scaling of plant energetics and population density. *Nature* 395:163–165.
66. Kempes CP, Wang L, Amend JP, Doyle J, Hoehler T (2016) Evolutionary tradeoffs in cellular composition across diverse bacteria. *ISME J* 10:2145–2157.
67. Tilman D (1981) Tests of resource competition theory using four species of lake michigan algae. *Ecology* 62:802–815.
68. Dutkiewicz S, Follows MJ, Bragg JG (2009) Modeling the coupling of ocean ecology and biogeochemistry. *Global Biogeochem. Cycles* 23:1–15.
69. Barton AD, Dutkiewicz S, Flierl G, Bragg J, Follows MJ (2010) Patterns of diversity in marine phytoplankton. *Science* 327:1509–1511.